

Parametric study of shock-induced transport and energization of relativistic electrons in the magnetosphere

J. L. Gannon and X. Li

Laboratory for Atmospheric and Space Physics, University of Colorado, Boulder, Colorado, USA

M. Temerin

Space Sciences Laboratory, University of California, Berkeley, Berkeley, California, USA

Received 11 July 2004; revised 4 August 2005; accepted 12 September 2005; published 9 December 2005.

[1] The sudden appearance of a new radiation belt consisting of electrons with energies greater than 13 MeV near 2.5 Earth radii (R_E), was observed by CRRES (Combined Radiation and Release Experiment Satellite) on 24 March 1991. Li et al. (1993) showed that the cause was an electromagnetic pulse within the Earth's magnetosphere caused by an unusually strong, fast shock in the solar wind. Sudden shock-induced injections of electrons with energies above 10 MeV to equatorial distances within 2.5 R_E are extremely rare because of the intensity of the shock required. In the current study, the propagation velocity parameter and electric field amplitude of pulses within the magnetosphere in the Li et al. model were varied from 750 to 2500 km/s and 70 to 400 mV/m, respectively. It was found that a stronger electric field shifted the peak of the resultant relativistic electron population toward the Earth. Doubling the electric field amplitude from 120 to 240 mV/m moved the peak of the injected electrons with energies above 13 MeV from 2.8 to 2.4 R_E . However, as the electric field pulse becomes even larger, the increase in response diminishes. This asymptotic behavior shows that it is extremely difficult to produce energetic electron injections inside two Earth radii. The nominal propagation velocity (velocity parameter) is compared to the radial propagation velocities that would have been measured under this model and others and compared to observation. It is found that although the model radial velocity is smaller than the velocity parameter and decreasing with radial distance, it is faster than MHD results and observations. Decreasing the nominal propagation velocity of the pulse within the magnetosphere from 2500 km/s to 1400 km/s also moved the peak of the injected electrons with energies above 13 MeV slightly closer to the Earth. However, at velocities smaller than approximately 1200 km/s the number of electrons injected within 2.5 Earth radii with energies above 13 MeV greatly decreased. Halving the velocity from 2000 to 1000 km/s shifted the peak of electrons with energy greater than 13 MeV from $L = 2.6$ to $L = 2.4$ but produced a count rate reduced by a factor of more than 250, resulting in no significant new radiation belt. These results show that the typical large electromagnetic impulses caused by interplanetary shocks, with amplitudes of the order of 10 mV/m, are more than an order of magnitude too small to produce any significant new radiation belts within 2.5 Earth radii with energies of the order of 10 MeV. Contributing to the difficulty in producing such a new belt is the need for an already relativistic electron population with adequate flux beyond geosynchronous orbit. These results thus also help explain the rarity of events such as the 24 March 1991 injection.

Citation: Gannon, J. L., X. Li, and M. Temerin (2005), Parametric study of shock-induced transport and energization of relativistic electrons in the magnetosphere, *J. Geophys. Res.*, 110, A12206, doi:10.1029/2004JA010679.

1. Introduction

[2] There are several known processes for particle energization in the magnetosphere that can create radiation belts.

It has not yet been determined which process dominates, but each has been shown to explain different phenomena. Radial diffusion, which occurs over a time scale of days, energizes electrons by bringing them inward from larger L shells [e.g., Schulz and Lanzerotti, 1974; Selesnick et al., 1997; Li and Temerin, 2001]. Processes that are μ (magnetic moment)-breaking, such as local heating, have also been

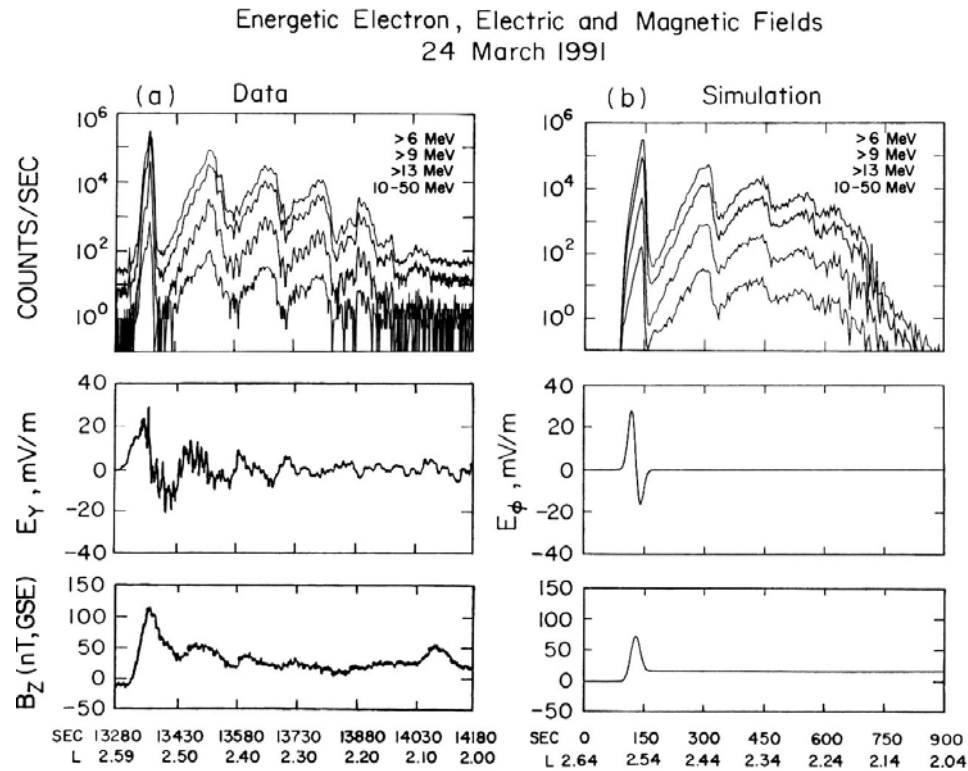


Figure 1. (a) Electron count rate and field measurements from the CRRES satellite. (b) Simulation fields and results from *Li et al.* [1993]. (Taken from Figure 1 of *Li et al.* [1993]).

explored, for example the in situ heating of electrons by VLF waves on the same L shell [e.g., *Temerin et al.*, 1994; *Summers et al.*, 1998; *Horne and Thorne*, 1998; *Meredith et al.*, 2001, 2002; *Albert*, 2002]. This paper focuses on shock-induced acceleration, a μ -conserving process that can produce significant acceleration within a minute.

[3] On 22 March 1991, an optical flare was observed on the Sun [*Blake et al.*, 1992]. Twenty-eight hours later, 24 March 1991, the effects of the associated interplanetary shock were seen by the CRRES satellite, which was fortuitously located at approximately $2.5 R_E$, during its inbound pass on the nightside near the equatorial plane. Immediately after the shock hit the Earth, CRRES observed a very rapid (<1 min) four order of magnitude increase in very energetic electron and ion fluxes, as well as a bipolar electric field and unipolar magnetic field pulse (see Figure 1a). The CRRES data showed the initial injection and subsequent drift echoes of the electrons as they drifted around the Earth and back to the detector. From the clear, 150 second drift period between these peaks, *Blake et al.* [1992] inferred that the injected electrons had energies with a peak around 15 MeV, otherwise more dispersion of the drift echoes would have been seen and that the energy of most of the electrons was greater than 13 MeV since all integral channels below that energy measured essentially the same flux.

[4] Impulses from the solar wind and the subsequent reactions of magnetospheric particle distributions are common and often observed [e.g., *Wilken et al.*, 1982; *Araki et al.*, 1997; *Lorentzen et al.*, 2002] but usually the effects on particle distributions of such impulses are observed at larger

distances from the Earth near geosynchronous orbit and at lower energies than those of the 24 March 1991 event [*Li et al.*, 2003]. However, though adequate observation to differentiate between the effects of shock-induced energization and the effects of the main phase of a storm is not often available, events similar to the 24 March event may not be unique in the observational record. In the early 1960s, *McIlwain* reported a new 4–100 MeV proton belt at a radial distance of $2.2 R_e$ from the 1962 data of Explorer XV, the actual formation of which was not observed. Such large events are rare but important because of the magnitude and duration of the effect on our Earth's space environment. It is unknown exactly how long the effects of the event *McIlwain* observed persisted, however the effects of the 24 March 1991 event were observed by SAMPEX for almost 10 years [*Li and Temerin*, 2001]. In recent times, there have been observations of energetic particle injections deep into the inner magnetosphere, associated with sudden solar wind variations and subsequent magnetospheric storms. For example, *Lorentzen et al.* [2002] described several energetic ion and electron injections observed by SAMPEX, Polar and HEO spacecraft which occurred in 1998 and 2000. None of these events produced the dramatic results of the 24 March event, and we cannot be certain whether they are due to sudden impulses or associated with geomagnetic storms, which also produce increased particle fluxes, without observation of the energization and concurrent field measurements.

[5] Because the observational record is relatively short, we do not yet know the full possible range of solar activity and its effects on the magnetosphere. Thus the sudden

injection of 15 MeV electrons and even more energetic ions to $L = 2.5$ on 24 March 1991 was extremely surprising. More recently, the activity known as the ‘‘Halloween Storm’’ during solar activity in late October and November 2003 caused the Earth’s radiation belt electrons to peak around $2\text{--}3 R_E$. This distortion was maintained for many days, corresponding to a reduced and contracted plasmasphere [Baker *et al.*, 2004]. In addition, following the Halloween storm, a new population of ultrarelativistic electrons (>10 MeV) appeared centered around $2 R_E$, and persisted to the end of the SAMPEX mission, as a striking change to the electron population in the radiation belts [Looper *et al.*, 2005]. That surprising large events can occur is also emphasized by the recent reanalysis of the so-called superstorm of 1859 by Tsurutani *et al.* [2003] and Li *et al.* [2005]. If their analyses are correct, it implies that the magnitude (about -1700 nT) of the 1859 storm as measured by the *Dst* index was almost three times larger than any in the recent historical record dating back to 1957 (the largest, -589 nT on 14 March 1989). The sudden storm commencement (SSC) for the 1859 storm occurred about 17 hours after the observation of a large solar flare suggesting an average interplanetary shock velocity of about 2400 km/s between the Sun and the Earth, substantially faster than the 24 March 1991 shock. In this paper we focus on the rapid energization and transport of radiation belt electrons associated with a sudden impact on the magnetosphere from such large interplanetary shocks.

[6] One unique aspect of the 24 March 1991 event was the availability of in situ simultaneous measurements of electric and magnetic fields [Blake *et al.*, 1992] and particles from CRRES, which provided a basis for comparison to simulation. Li *et al.* [1993, 1996] and Wygant *et al.* [1994] interpreted these data. Under their interpretation, an interplanetary shock from the sun impacted the Earth’s magnetosphere producing an electromagnetic wave within the magnetosphere that drove electrons and ions inward.

[7] The sudden electron enhancements from this event were modeled by Li *et al.* [1993]. The results of the simulation reproduced the observation (see Figure 1b) and explained the mechanism of shock-induced radial transport and energization of electrons. Later, Hudson *et al.* [1995] successfully used the same model to reproduce the observed sudden proton enhancement. Elkington *et al.* [2002] ran a guiding-center electron simulation of the event using MHD model fields, resulting in a peak in the energy spectrum at about 13 MeV around $L = 3$. However, these works study only one event. In this study, we explore the effect that changes in the parameters of this model, representing different shocks and/or magnetospheric conditions, have on the acceleration of highly relativistic electrons.

[8] To understand how the shock affects a population of energetic particles, one can first look at the effect of the shock on a single particle. If the Earth’s magnetosphere is suddenly compressed by the shock wave, Faraday’s law gives an electric field primarily in the azimuthal direction in the equatorial plane.

[9] Energization can be achieved through two terms under the guiding center approximations (equation (1)) [Northrop, 1963]. Both terms comparably contribute to

energization of the electrons. One of those terms represents betatron acceleration, and the other includes $\mathbf{E} \cdot \mathbf{v}_d$, electron drift antiparallel to the electric field. Looking at the guiding center approximations for equatorially mirroring particles, we see from the first term in equation (1) that an eastward drifting electron interacting with the westward pointing electric field of the incoming wave is energized, whereas an electron interacting with the oppositely oriented electric field of the outgoing wave is deenergized. The second term, the betatron term (also referred to as the induction term), is related to the curl of the electric field, and also leads to energization or deenergization of the electron, as the magnetic field either increases or decreases.

$$\dot{W} = e\dot{\mathbf{R}}_{\perp} \cdot \mathbf{E} + \frac{\mu}{\gamma} \frac{\partial B}{\partial t} \quad (1)$$

$$\dot{\mathbf{R}}_{\perp} = \frac{\hat{e}_1}{B} \times \left(-c\mathbf{E} + \frac{\mu c}{e\gamma} \nabla B \right), \quad (2)$$

where W is energy, R is radial position, e is electron charge, E is electric field, B is magnetic field, \hat{e}_1 is the unit vector in the direction of the magnetic field, c is the speed of light, and μ is the first adiabatic invariant.

[10] Equivalently, we can consider the energization in terms of conservation of the first adiabatic invariant (magnetic moment) of the particle. In order to conserve the first adiabatic invariant, as a particle moves closer to the Earth to a region of higher magnetic field, it gains energy (equation (3)). The first adiabatic invariant should be conserved for this process because the time scale of the injection is about a minute, much longer than the gyroperiod of an electron. For a relativistic electron, the first adiabatic invariant is

$$\mu = \frac{p_{\perp}^2}{2m_0B}, \quad (3)$$

where μ is the first adiabatic invariant, $p_{\perp} = \gamma m_0 v_{\perp}$ is the perpendicular component of the particle’s momentum, B is magnetic field, and m_0 is the particle’s rest mass. A particle that interacts more strongly with the incoming (compression) pulse than the outgoing (relaxation) pulse will remain at a lower L value and be energized. A preferentially energized particle will have a drift velocity that allows it to stay in phase longer with the compressive wave. Also, for a pulse whose strength depends on local time, the initial position of a particle determines the strength of the incoming and reflected pulse seen by the particle. Therefore the electron that is most affected must begin at a local time such that it sees the strongest part of the compression and the weakest part of the relaxation.

[11] This study uses the Li *et al.* model as the basis for the parametric study investigating shock-induced energization. It reproduced well the electron count measurements for the 24 March 1991 event, the one event for which we have good flux and field measurements at the time of the injection. Using a guiding center code to follow electron trajectories in the model allows us to efficiently use computing time. As in the original work by Li *et al.* [1993], we only trace equatorially mirroring particles. The electric field

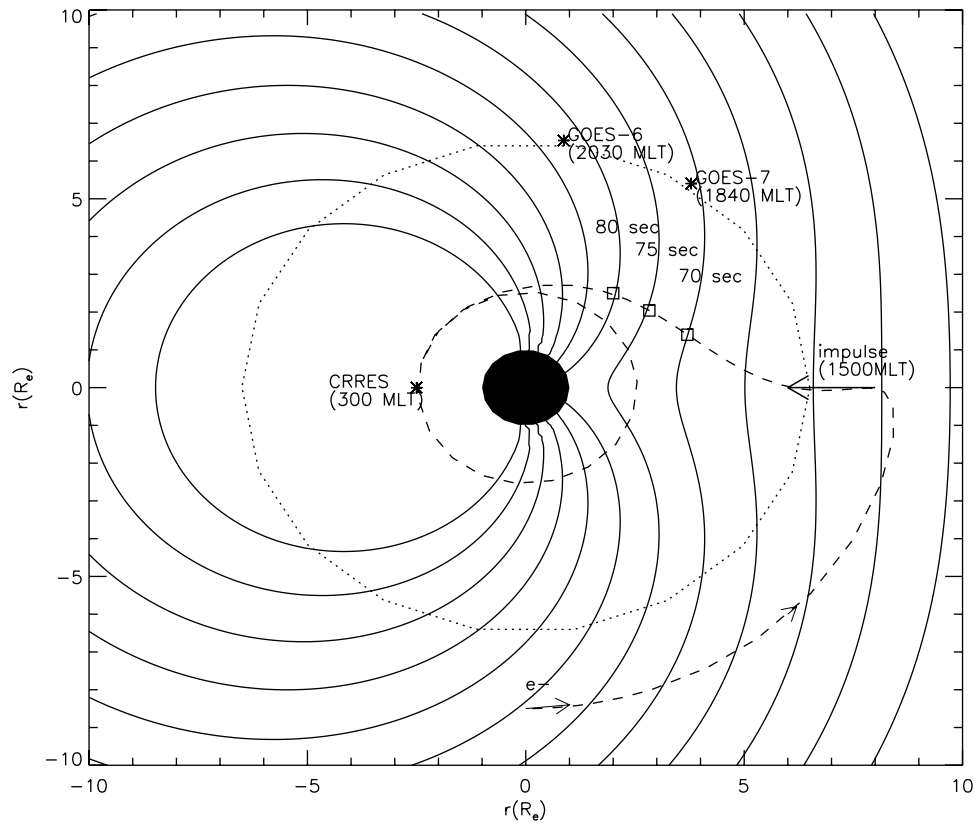


Figure 2. Wavefront propagation of the incoming pulse of the electric field used in the model, $v_0 = 2000$ km/s, $E_0 = 240$ mV/m. The wavefront is shown at 5 s intervals from event onset. The positions of CRRES and the GOES satellites are marked by a star symbol. The drift path of an example energized electron beginning at $L = 8.5$ is shown by the dashed line, and its position at time = 70, 75, and 80 s is marked.

is modeled as an incoming and reflected pulse field, as follows:

$$\mathbf{E}(r, t) = -\hat{e}_\phi E_0 (1 + c_1 \cos(\phi - \phi_0)) (e^{-\xi^2} - c_2 e^{-\eta^2}) \quad (4)$$

$$\begin{aligned} \xi &= [r + v_0(t - t_{ph})]/d \\ \eta &= [r - v_0(t - t_{ph} + t_d)]/d \\ t_{ph} &= t_i + \left(\frac{c_3 R_e}{v_0}\right) [1 - \cos(\phi - \phi_0)]. \end{aligned}$$

The exponential terms represent the compression and relaxation of the magnetosphere as oppositely directed gaussian pulses. The exponents of the gaussians include a time delay. The exponential form is multiplied by a local time modulation, with the strongest point of the electric field corresponding with the point of impact of the impulse. The electric field looks like a wave, propagating inward and azimuthally, and partially reflecting at the ionosphere. The parameter $c_1 = 0.8$ affects the local time dependence, a nine-to-one ratio between the maximum at the point of impact and the minimum on the opposite side of the Earth, $c_2 = 0.8$ determines the amount of reflection, $c_3 = 8.0$ represents the magnitude of the propagation delay in the azimuthal

direction, $t_d = \frac{2.06 R_e}{v_0}$, the location of the reflection is $r = 1.03 R_e$, and $t_i = 81$ sec is the initial reference time. The radial velocity of magnetospheric propagation at the point of impact is represented by v_0 , $d = 30,000$ km is the width of the pulse, and $\phi_0 = 45^\circ$ (1500 magnetic local time) is the point of impact of the interplanetary shock on the magnetosphere, also the local time of largest electric field amplitude. The magnetic field is calculated using Faraday's law under vacuum assumptions. Using these parameters mimics the unipolar electric field and bipolar magnetic field observed by CRRES. It produces an electric field fluctuation that varies with local time. Therefore particles at different locations see different parts of the pulse and different field strengths. Particles traveling at different velocities interact with the field at magnitudes that change with time differently. Therefore an electron that originates in the right position to see the field magnitude maximum and drifts at the right speed to travel with that propagating peak would be energized more than an electron with a different speed or initial position.

[12] Figure 2 shows the propagation of a wavefront (incoming pulse only) at 5 s time intervals for the model with $v_0 = 2000$ km/s. The positions of GOES 6 and 7 and CRRES at the time of the event are marked by the star symbol and the trajectory of a typical electron (for $E_0 = 240$ mV/m) that contributes to the formation of the new

radiation belt around $L = 2.5$ is shown and marked by a square at the corresponding 5 s intervals. The electron begins at $L = 8.5$ with an energy of about 1.5 MeV, drifts around the Earth to encounter the pulse at its onset, is energized and moves in to $L = 2.5$ with a final energy of about 13 MeV. The magnitude of the velocity parameter, v_0 , corresponds to the radial velocity of the pulse at a given local time. More important, however, is the propagation velocity of the pulse in the direction of the drift of the electrons, which is not constant throughout the simulation region. The lines marking 5 s intervals become further spread apart as the velocity decreases. As can be seen in the figure, there is an effective decrease of wavefront velocity with decreasing radial distance along the impact meridian. Along the particle trajectory (indicated by a dashed line in Figure 2), the 5-s intervals become closer, allowing an electron to stay in phase with the pulse maximum as it accelerates.

[13] The electron distribution used as the initial conditions in the simulation by Li et al. extended every $0.1 R_E$ from 3.0 to $9.0 R_E$, every three degrees in azimuth and every 10% in initial energy from 1.0 to 9.0 MeV. Only equatorially mirroring electrons are included. Because the electron distributions vary by many orders of magnitude, we introduce a weighting factor so that we can trace the same number of electrons at a particular set of initial conditions regardless of electron distribution. The weighting, as follows, was included to simulate a realistic source electron distribution, including a strong power law in energy, as well as a parabolic weighting in radial position, in order to reproduce the observation. The weighting was necessary because tracing all electrons in the energy and spatial ranges we desired was computationally unrealistic. We instead trace electrons representative of a distribution. In other words, in higher-density areas, we do not need to know how every electron acts, and we use the weighting to let one electron represent the response of the distribution around it while maintaining a proper count relative to other parts of the distribution. The L^2 term corrects for the increase in area of a wedge of two-dimensional phase space as radial distance increases.

$$\text{weighting} = G(L) * L^2 * w^{-7} * \frac{v}{v_d} \quad (5)$$

$$G(L) = 1 - \frac{(L - L_0)^2}{a_0}$$

$$a_0 = 7.5$$

$$L_0 = 10,$$

where L is equivalent to radial distance in units of Earth radii under a dipole model, w is energy, v is gyration speed at the point of measurement, and v_d is drift velocity at the point of measurement. The $\frac{v}{v_d}$ parameter corrects for the difference between the gyration speed measured by the detector and the drift-averaged velocity used to trace the guiding centers of the electrons in this simulation, rather than the complete motion.

[14] The energy weighting, w^{-7} (w^{-8} including the 10% steps in initial energy distribution), is quite steep, and was

necessary to match the flux levels observed by CRRES for the original event simulation.

2. Results and Discussion

2.1. Parametric Study

[15] The Li et al. model successfully reproduced the drift echoes and narrow energy spectrum of a single, unique event. We use it to study the response of the same source population to model changes by looking at possible high-energy radiation belt outcomes and at the effects of possible events even more extreme than that of 24 March 1991. Two parameters of the Li et al. model were varied, representing varying shocks and/or magnetospheric conditions, E_0 , which is the amplitude of the electric field pulse, and v_0 , which is the propagation speed parameter.

[16] The electric and magnetic fields of the pulse and pulse propagation velocity cannot really be varied independently. Inspecting Faraday's law under a simple plane wave assumption reveals the following:

$$\frac{\partial \mathbf{B}}{\partial t} = -c \nabla \times \mathbf{E} \quad (6)$$

$$\Rightarrow -i\omega B = -cikE$$

$$\Rightarrow v \propto \frac{E}{B},$$

where B is magnetic field, E is electric field, k is the wave vector, and c is the speed of light. Increasing the electric field requires an increase in either velocity or magnetic field. Similarly, increasing the velocity necessarily increases the electric field or decreases the magnetic field magnitude of the pulse, under this assumption. The two scenarios we looked at were varying electric field, keeping pulse velocity constant, and varying pulse velocity, keeping magnetic field constant.

[17] We quantified the effect of the variations by looking at the radial position of the peak of the resultant population and the flux at that peak. For example, Figure 3 shows our results for electrons greater than 13 MeV using the original parameters from the Li et al. simulation of the 1991 event, and Figure 4 shows a simulation using a values of v_0 and E_0 that are about half as large. The contours in the top plot are approximately logarithmic, varying about an order of magnitude per contour. Note that these plots are used for determination of spatial and temporal locations only, so the contour levels are different in each plot. The lobes are the first injection and subsequent drift echoes. As time progress, dispersion can be seen, as different energy electrons drift at different speeds. In this example, as v_0 and E_0 decrease, electrons at higher L shells contribute less and the radial location of the point of highest electron flux, L_{peak} , appears to shift from $2.5 R_E$ to $2.2 R_E$. The flux at the respective peaks also drops by a factor of more than 250. In this example, the lower velocity and electric field amplitude case essentially produces no radiation belt of significance.

2.2. Variations in E_0 and B , Constant Velocity

[18] The first parameter we chose to study was the amplitude of the electric field of the pulse (70 to

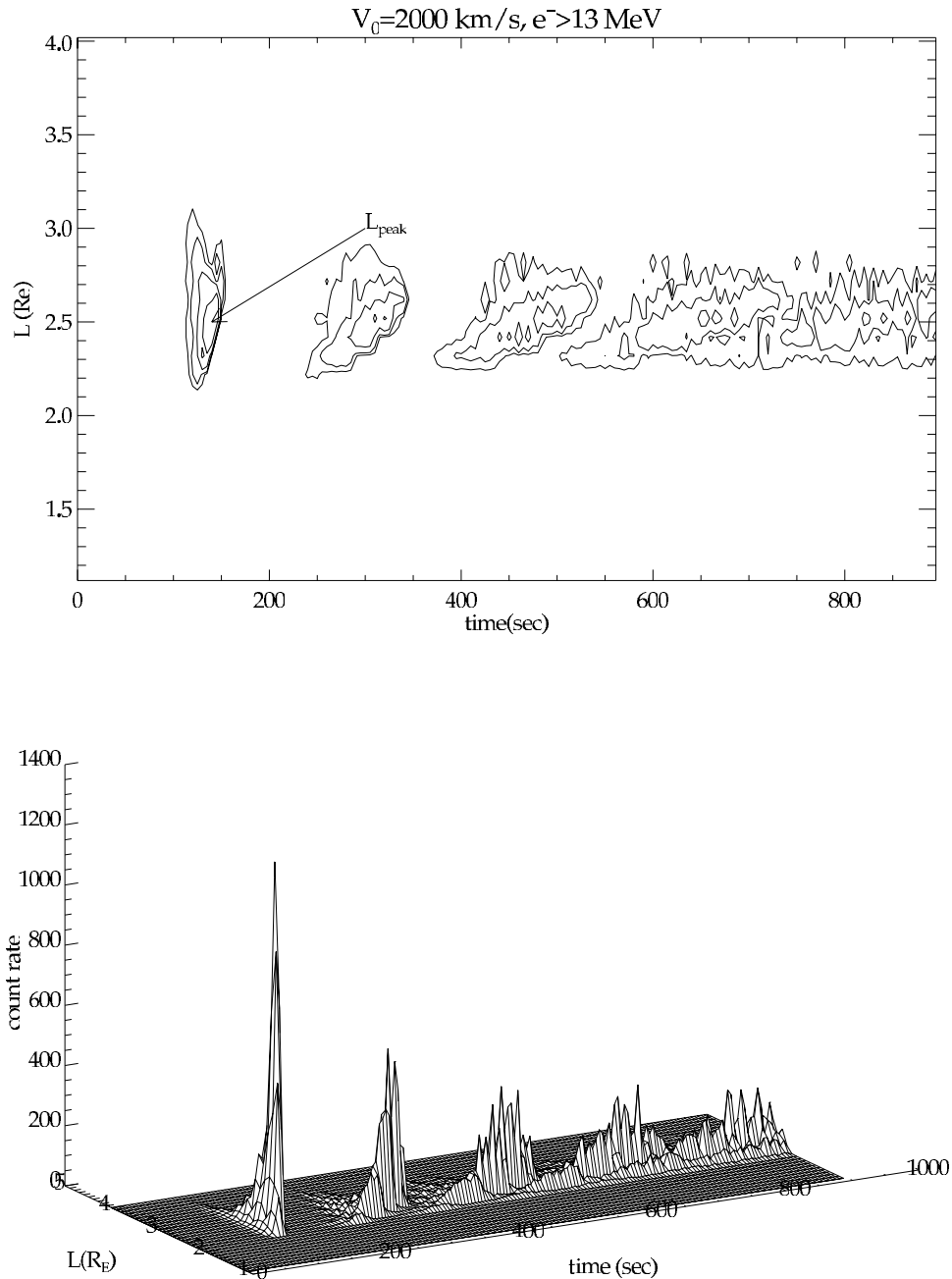


Figure 3. Two views of electron count rate, energies greater than 13 MeV, from simulation results using the same parameters as for the 24 March 1991 simulation, $v_0 = 2000$ km/s, $E_0 = 240$ mV/m. In the top plot, the x-axis is time in seconds, the y-axis is radial position, in R_E , and the contours represent log (electron count rate).

400 mV/m) while keeping the pulse velocity constant and thereby also varying the magnetic field. Because this is a wave-resonant process, keeping a constant velocity selects approximately the same resonant electron population. We are looking at the effect of a bigger pulse on similar particles. A larger amplitude electric field represents a larger and/or sharper interplanetary shock, in velocity or particle density, leading to a faster compression. An increase in the magnitude of the electric field correspondingly increases the amount of energy gained by the electrons, other parameters remaining the same. We ran the simulation with different

values of E_0 . Figure 5 summarizes the results of several runs under varying amplitudes. For each run, we traced approximately 300,000 electrons, the same source population as used under the Li et al model for the 24 March 1991 event. As an electron passed a selected local time (in our case, directly opposite the point of impact, $\phi - \phi_0 = 180^\circ$), we recorded its radial position, energy, time, identification number, and calculated weighting factor. For each run, we found the final peak position and count rate level for electrons for various energy ranges, including energy greater than 13 MeV (Figure 5). A larger electric field yields a peak

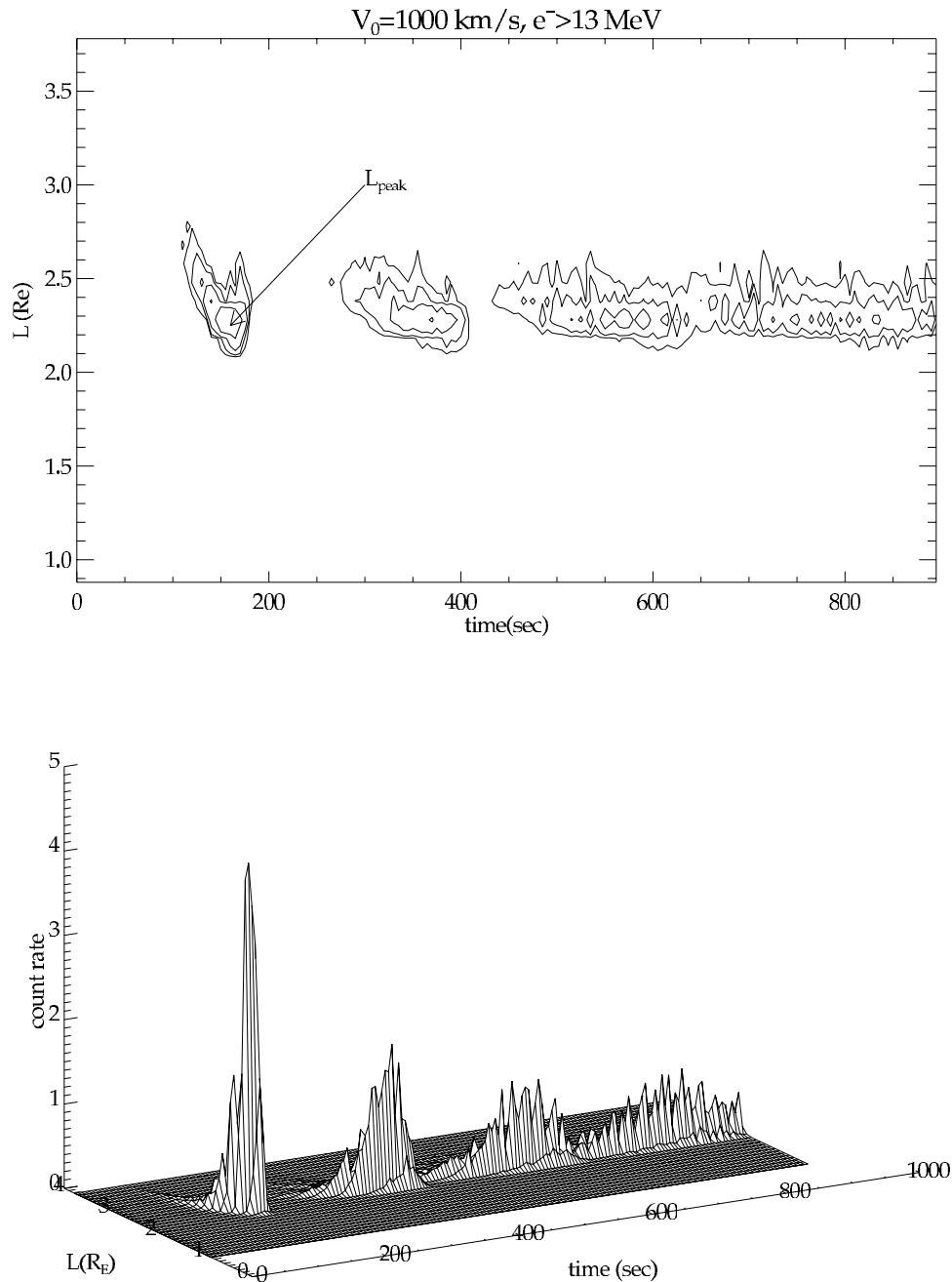


Figure 4. Same as Figure 3, except $v_0 = 1000$ km/s, $E_0 = 120$ mV/m. This plot is used for comparison of peak position only, so note that contours are different than in Figure 3. For electron count comparison, refer to Figures 5 and 6.

closer to the Earth, and more counts at that peak. This is consistent with *Wygant et al.* [1994], who showed that electric fields of 200–300 mV/m are required to bring electrons to where CRRES observed them at $L = 2.5$ from L shells greater than seven. They also showed that as $\langle E\delta t \rangle$ became larger, electrons were energized more and brought in from farther.

2.3. Variations in v_0 and E, Constant B

[19] The other parameter we chose to vary was the propagation velocity parameter (750 to 2500 km/s), which is the magnitude of the radial velocity at the point of impact.

It can be a function of the interplanetary shock, particle densities, and local magnetic field strengths within the magnetosphere.

[20] In varying the velocity of the pulse, we chose to keep the magnetic field magnitude constant and allowed the electric field to increase with pulse velocity. We did this because magnetic fields are more commonly measured, so keeping a constant magnetic field in the parametric study facilitates comparison with data.

[21] The results of varying the propagation velocity are more complicated than pulse field amplitude variations, due to the resonant nature of the process. The resonance can be

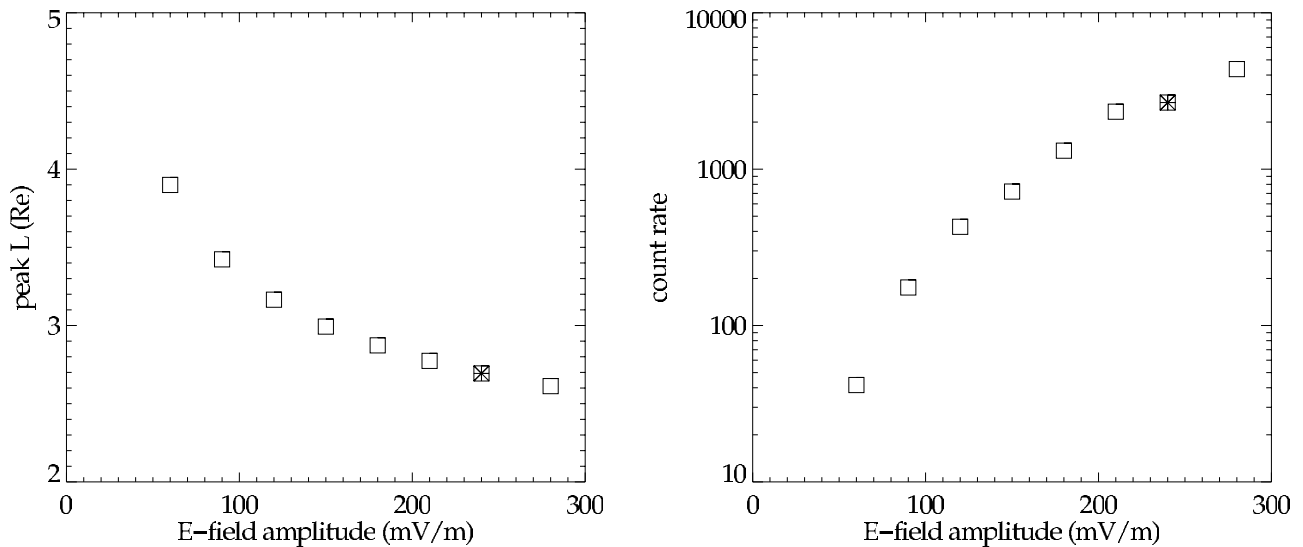


Figure 5. Simulation result summary vs amplitude of modeled electric field for electrons greater than 13 MeV. The left panel shows the location of resultant peak position. This is the radial position of the highest point of flux for a set of parameters ($\delta L = 0.1$). The right panel shows the relative countrate level at the above peak position. The star symbol denotes the parameters used to simulate the 24 March 1991 event.

described as particles “surfing” on the wave, thereby interacting with the strongest part of the wave the longest. Owing to the local time dependence of the pulse field, the most energized electrons are those that interact with the incoming pulse on the dayside and the outgoing pulse on the nightside. Decreasing the pulse velocity thereby preferentially selects lower-energy electrons, those that drift more slowly azimuthally. However, it also increases the time of interaction with the pulse. In addition, a slower velocity with a constant magnetic field implies a weaker electric field, which we previously showed decreases the effect on electrons.

[22] The results of the simulation (see Figure 6) show that as the pulse velocity becomes slower, the final radial location of the peak is pushed closer to the Earth, despite the decrease in the electric field. However, for the same source population as in the work of *Li et al.* [1993], the counts in the peak drop off quickly below about 1200 km/s (corresponding to $E_0 = 120$ mV/m). At these lower velocities, the peak consists of energized electrons that were already close to the Earth and thus already energetic but with small count rates. In fact, at the lower velocities, the peak of maximum flux has very few particles at all. These results show that the typical large electromagnetic impulses

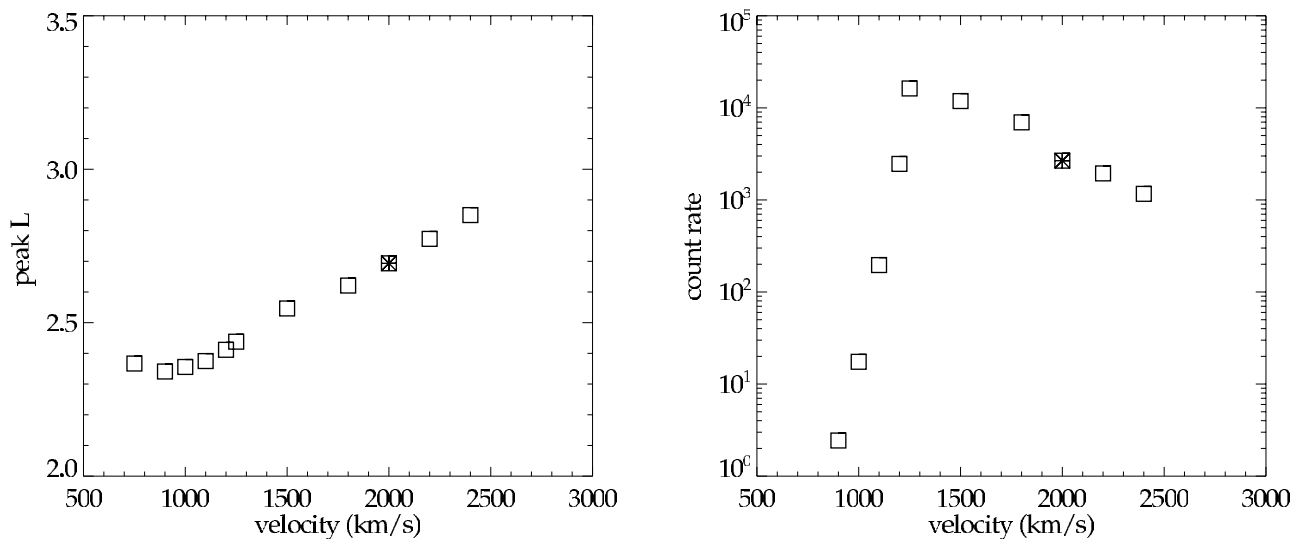


Figure 6. Same as Figure 5, varying v_0 instead of E_0 . The star symbol denotes the parameters used to simulate the 24 March 1991 event.

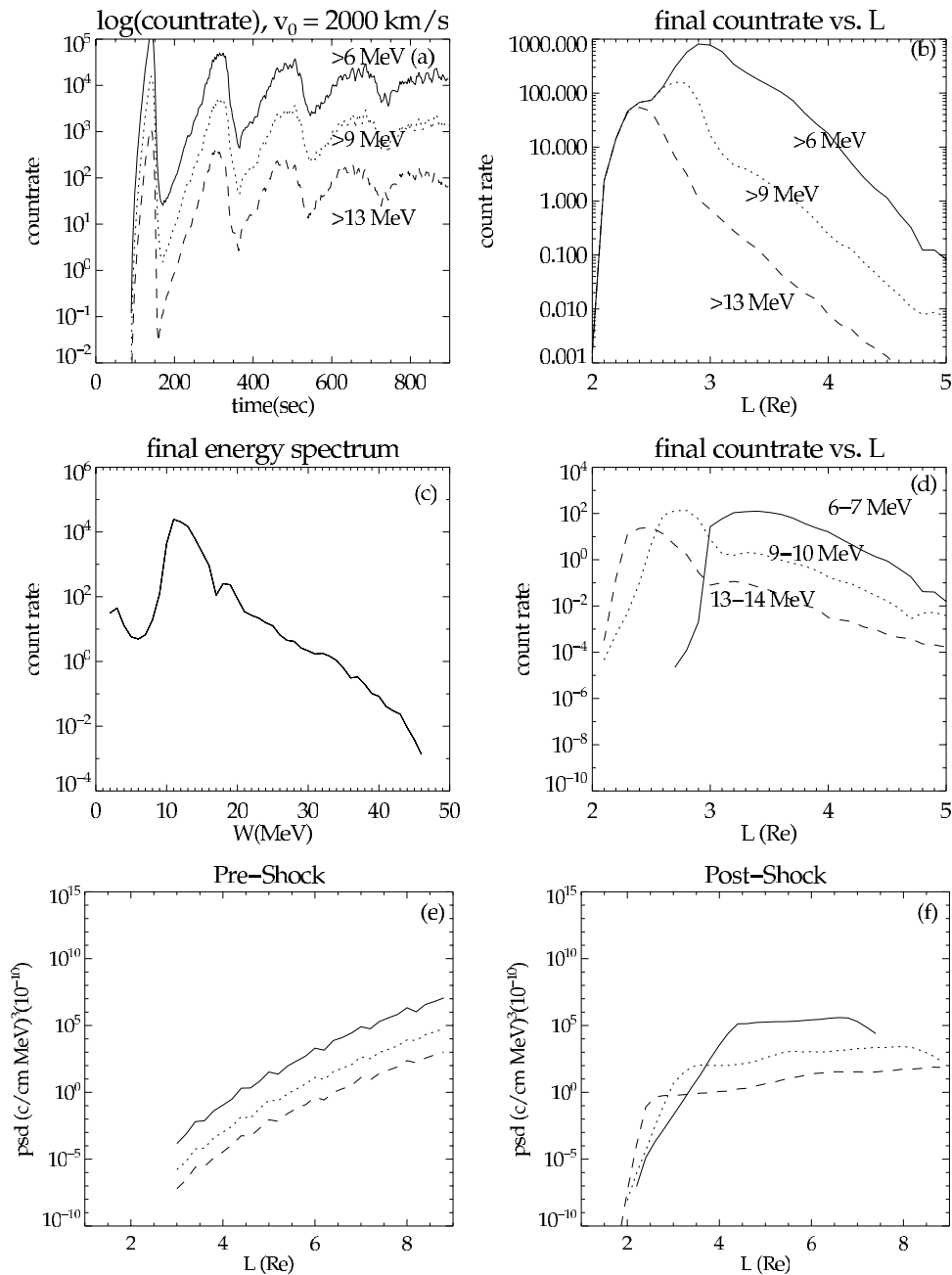


Figure 7. Simulation results for $E_0 = 240$ mV/m, $v_0 = 2000$ km/s. (a) Count rate at the peak of the >13 MeV distribution, $L_{peak} = 2.53$, $\delta L = 0.1$. (b) Final position distribution for each of three virtual integral energy channels. (c) Final energy spectrum at $L_{peak} = 2.53$. (d) Final position distribution of electrons under the simulation in three discrete energy ranges. (e) Preshock phase space density profile (solid: $\mu = 2077$ MeV/G, dotted: $\mu = 11,852$ MeV/G, dashed: $\mu = 45,898$ MeV/G). (f) Postshock phase space density profile (solid: $\mu = 2077$ MeV/G, dotted: $\mu = 11,852$ MeV/G, dashed: $\mu = 45,898$ MeV/G).

caused by interplanetary shocks, with amplitudes of the order of 10 mV/m (with velocities on the order of 100 km/s in this model), are more than an order of magnitude too small to produce any significant new radiation belts within 2.5 Earth radii with energies of the order of 10 MeV.

[23] Generally, the final population of electrons depends on the initial population, which is often not well measured. In the case of 24 March, although the higher-energy

differential (four channels from 1239 to 1633 keV) channels of the CRRES MEA (Medium Electron A) instrument were contaminated by ions, we can infer the level of flux by considering that the trends of higher-energy channels often follow those of the lower. In other words, if there is an increase or decrease in flux at one energy, there is most likely a similar variation at other energies. The lower-energy channels, just before the event onset, showed a slight

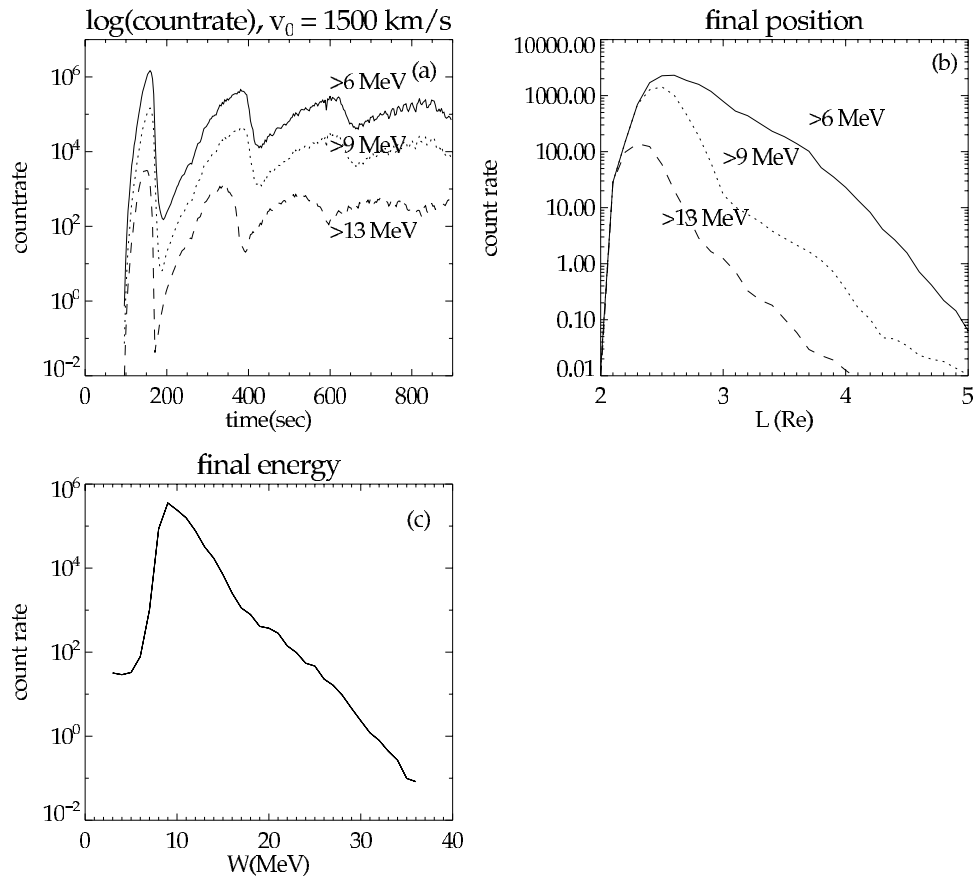


Figure 8. Simulation results for $E_0 = 180$ mV/m, $v_0 = 1500$ km/s. (a) Count rate at peak location of >13 MeV electron distribution, $L_{peak} = 2.44$, $\delta L = 0.1$. (b) Final position distribution for each of three virtual integral energy channels. (c) Final energy spectrum at $L_{peak} = 2.44$.

elevation in flux levels compared to previous measurements, possibly due to enhanced geomagnetic activity several days prior. From this, we infer that the flux of 1–2 MeV electrons before the arrival of the shock was most likely above average but within the normal range. Therefore it seems that the strong response to this event is explained by the uniqueness of the shock, rather than the uniqueness of the preexisting electron source population. In recent work by *Blake et al.* [2005], comparisons of several large events are made, showing that strong storms do not always correlate the persistence of a new population of particles, which they suggest requires an injection to low L , and is usually associated with unusually rapid rise times.

[24] In addition, as the velocity of the pulse decreases, electrons from farther away no longer reach the inner magnetosphere. For example, in the original event, the bulk of the electrons observed by CRRES were shown to originate at 7–9 R_E . At half the original velocity, the electrons originate at 5–6 R_E . (Electrons from 5–6 R_E were also present in the original event but only contributed to a relatively small portion of the final flux.) Therefore they have a smaller radial distance to travel, and a smaller gain in energy. Figures 7, 8, and 9 show a summary, for $v_0 = 2000$ km/s, $v_0 = 1500$ km/s and $v_0 = 1000$ km/s, of flux measurements at the peak of the >13 MeV final electron distribution ($L_{peak} = 2.53, 2.44,$ and $2.43,$ respectively) for

three different energy channels (Figure 7a), the final count rate versus L of electrons for those energy channels (Figure 7b), and the final energy spectrum of all electrons that would be encountered at L_{peak} (Figure 7c). In addition, the fastest velocity case, which is representative of the 24 March 1991 event, includes the final count rate distribution of electrons in the selected discrete energy ranges, 6–7 MeV, 9–10 MeV, and 13–14 MeV (Figure 7d), and the phase space density profiles versus L calculated from the simulation output preshock (Figure 7e) and postshock (Figure 7f) [*Gannon and Li, 2005*].

[25] The three phase space density curves include electrons at a specified value of the first adiabatic invariant, $\pm 10\%$, corresponding to a 6 MeV, 9 MeV, and 13 MeV electron at 2.5 R_E . In the count rate versus time plots of Figure 7, the drift echoes for the three channels are coincident in time, which implies the bulk of the electrons have energies above the highest threshold, i.e., greater than 13 MeV. In the slowest velocity case, Figure 9, the drift echoes for the >6 MeV and >9 MeV channel are coincident, but in the >13 MeV channel they appear more often, with much lower count rate, implying that there are some electrons in this case that are seen by both the lower channels but not the upper, i.e., between 9 and 13 MeV. This is verified by looking at Figure 7c; the peak of the final energy spectrum is lower for the slower velocity case.

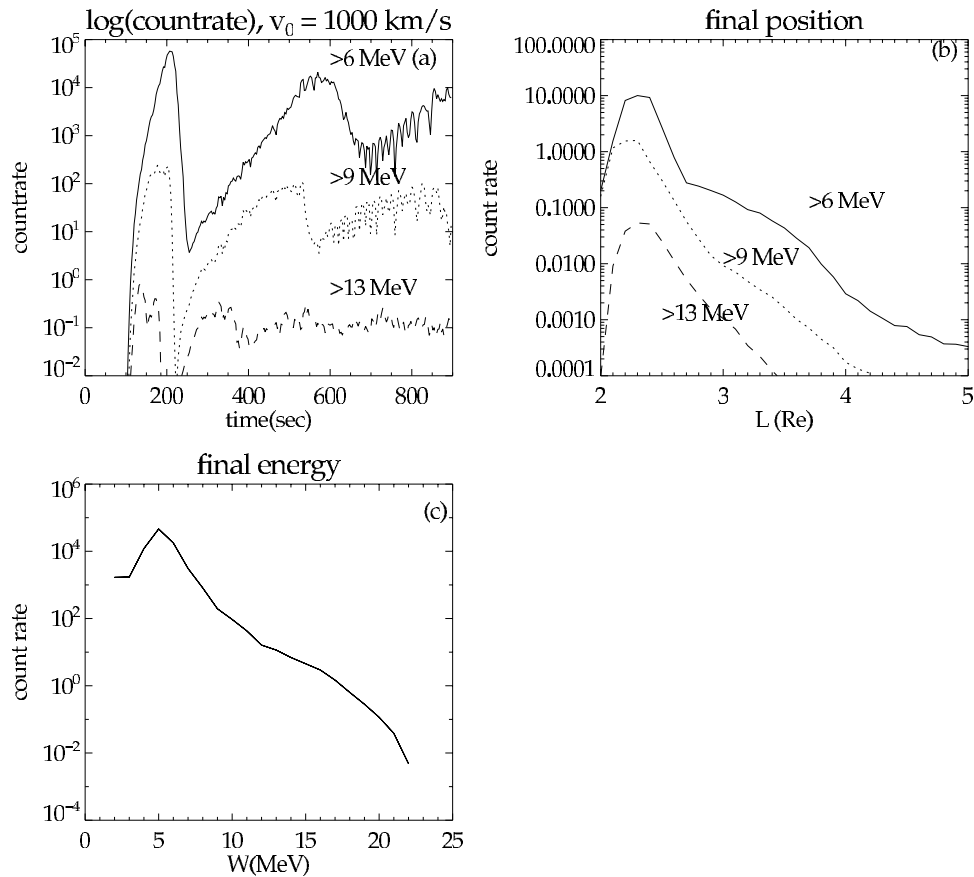


Figure 9. Simulation results for $E_0 = 120$ mV/m, $v_0 = 1000$ km/s. (a) The $\log(\text{count})$ at peak location of >13 MeV electron distribution, $L_{\text{peak}} = 2.43$. (b) Final position distribution for each of three virtual integral energy channels. (c) Final energy spectrum at $L_{\text{peak}} = 2.43$.

[26] In the slower velocity case, the energized electrons at $L = 2.5$ originate closer to the Earth. Thus electrons at higher L shells contribute less, resulting in the appearance of an earthward shifted peak and, because the electrons travel a smaller radial distance, they gain less energy resulting in a less energetic final energy distribution. The velocity used in Figure 8, 1500 km/s, corresponds to the propagation speed that the parametric study suggests is most effective in moving energetic (10 MeV) electrons earthward to produce a significant flux level (Figure 6). From the coincident drift echoes at a detector location of $2.44 R_E$ in Figure 8a, similar to Figure 7a, we see that a large portion of the electrons remain above 13 MeV. Looking at Figure 8b, we see that the contribution from electrons greater than 9 MeV appears to peak at a lower L value. Figure 8c confirms that the final energy spectrum peaks at a lower energy, approximately 9–10 MeV, than the 2000 km/s case, which peaked at 12–13 MeV (Figure 7c). This implies that in order to reproduce the energies observed by CRRES, this type of model required the higher pulse propagation velocity. This could possibly be offset by a larger pulse width, or properly varying velocity, but, as is discussed later, the correct velocity variation is not fully agreed upon, and even the simplest explicit variations with radial distance makes the study computationally less feasible. We hope to glean physical insight from this simplified model which is able

to reproduce several important facets of known events, keeping in mind that other factors may contribute.

2.4. Minimum L Reached

[27] We wished to determine how close to the Earth a new radiation belt can be injected by a shock. Figure 10 shows the minimum L value reached by a ring of electrons with a range of initial energies from 1 to 9 MeV, beginning at a particular radial distance ($L = 5, 7, 9 R_E$), versus their first adiabatic invariant. They were traced in the same model field as the original *Li et al.* [1993] work ($E_0 = 240$ mV/m, $v_0 = 2000$ km/s). Work done by *Elkington et al.* [2002] showed similar results achieved by tracing electrons in MHD fields. Comparing fast and slow propagation velocities further explores the requirements for resonance (see Figure 11). For the 2000 km/s case, the lowest L value reached in Figure 11 is by electrons with μ -values corresponding to an initial energy of about 1.5 MeV at $7.0 R_E$, which is consistent with our previous results (Figure 7). As the ring of electrons begins closer to the Earth, the minimum L value occurs for electrons of higher initial energies, as required to satisfy drift resonance with the wave velocity. For the 1500 km/s case, the resonant energy decreases compared to the faster velocity case and the minimum L value reached is closer to the Earth. This shows that the energies of the particles reaching the mini-

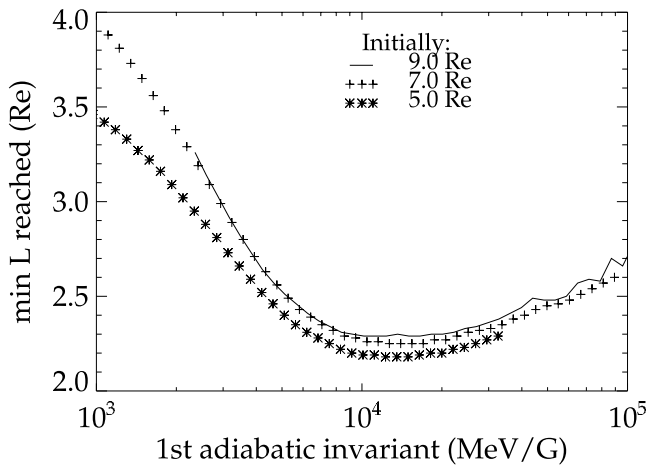


Figure 10. Minimum L value (R_E) reached by any electron beginning in a ring of same initial radial position (the dashed line, plus symbols, and star symbols correspond to 9.0, 7.0 and 5.0 R_E , respectively), versus magnetic moment. The field parameters correspond to those in the original *Li et al.* [1993] work, $E_0 = 240$ mV/m, $v_0 = 2000$ km/s. To obtain each point on the plot, we run a ring of particles beginning at a particular L shell at the energy corresponding to the magnetic moment on the x-axis. The minimum L value reflects the one particle in the initial ring that reaches the lowest L shell.

imum L values are determined by their drift resonance with the wave.

2.5. Optimum Conditions

[28] Also of interest is the possibility of more extreme events, which would produce a new high energy electron radiation belt with even larger fluxes at lower L shells. Within the context of the model the final flux is proportional to the initial flux. Thus much larger final fluxes are possible if initially the outer radiation belt is at a much higher flux. The results of this study also suggest that, while the perturbation must be exceptionally large and fast, increasing the electric field amplitude does not inject electrons much past 2.5 R_E (see Figure 5). The position of the final flux peak asymptotes as the electric field amplitude increases. The optimum propagation velocity in our model for producing an extremely energetic (>10 MeV) electron radiation belt as near to the Earth as possible appears to be around 1400–1500 km/s (Figure 6), although the energy of the final population is decreased (see Figures 7c, 8c, and 9c).

2.6. Impulse Propagation: Magnetosonic Waves

[29] Perturbations in the magnetosphere, produced from impulses in the solar wind, propagate via MHD modes [Wilken et al., 1982]. Alfvén waves propagate along field lines, and the slow- and fast-mode magnetosonic waves carry the perturbations across field lines. The propagation speeds of these waves depend on local plasma properties and the magnetic field. Thus they vary with radial distance and local time, as well with geomagnetic activity. The magnetosonic speed also depends on ion pressure. The velocities are related as $v_{\text{slow}} < v_{\text{alfven}} < v_{\text{fast}}$. However, in this region of the magnetosphere, the fast magnetosonic

speed approaches the Alfvén speed, and the slow magnetosonic speed is near the acoustic speed. *Hudson et al.* [1997] explored a radial profile of the Alfvén speed through an MHD code. *Waters et al.* [2000] used average plasma data for different regions to calculate an Alfvén profile. The results of both were similar. The Alfvén speed is below 500 km/s in the plasmasphere, where density is high, and then rises at the outer edge of the plasmapause to its maximum value. As the magnetic field drops off with radial distance, so does the Alfvén speed. In the work by *Hudson et al.* [1997], the Alfvén velocity reaches a maximum of 1200 km/s at 5 to 6 R_E .

[30] Our model of the propagation of the pulse through the magnetosphere is greatly simplified and has some obvious unrealistic features such as the constant radial velocity at a given local time. An understanding of how this disturbance really propagated is not completely agreed upon. *Hudson et al.* [1997] were able to trace energetic ions using fields generated by an MHD simulation of the 24 March 1991 event and reproduced some features of sudden particle injection and derived velocities similar to the Alfvén profiles previously mentioned. This suggests that the perturbation, while stronger than typical, could have propagated via standard MHD modes. In the 24 March event, the electrons producing the bulk of the final energetic electron flux at $L = 2.5 R_E$ were shown by *Li et al.* [1993], and also in the work of *Elkington et al.* [2002], to originate from about 7–9 R_E , where the Alfvén speed is normally less than 1000 km/s. However, our study suggests that fast magnetosonic waves, with velocities in the 500–1200 km/s range, are too slow to produce a significant new radiation belt with the observed drift echo features at $L = 2.5 R_E$. This presents a quandary, as two types of models, MHD and our simplified analytical model, were able to reproduce similar aspects of the same event with incompatible propagation velocities.

2.7. Impulse Propagation: Propagating Discontinuities

[31] A propagating discontinuity reflects the combination of quick magnetospheric compression, large $\frac{dB}{dt}$ and resulting

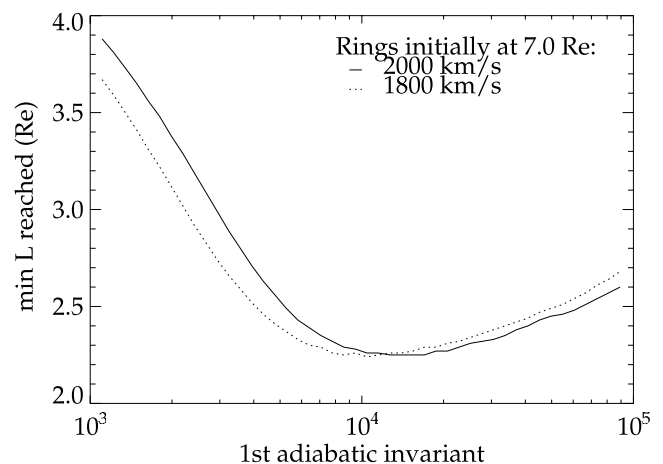


Figure 11. Comparison of minimum L values reached by a ring of electrons at 7.0 R_E initially, under different propagation velocities (keeping the magnetic field the same), versus magnetic moment.

inductive electric field, and fast propagation velocity required to reproduce the high final energy of the observed electron fluxes. A steepening of the velocity profile occurs due to nonlinear wave effects. As the first part of the disturbance passes a point, the local Alfvén speed is changed and a subsequent disturbance can travel faster, catching up with the initial one [Kunkel and Rosenbluth, 1966; Kennel *et al.*, 1985; Kantrowitz and Petschek, 1966]. Araki *et al.* [1997] also gives strong evidence of the uniqueness of the compression associated with the interplanetary shock of 24 March 1991. They suggest that the magnetopause was compressed on the order of “several tens of seconds,” as compared to typical compressions which occur on the order of minutes. On the basis of magnetopause crossings of satellites in geosynchronous orbit, they estimated the time of the compression and relaxation to be about 30 s. Lee and Hudson [2002] have shown that the shorter the time scale of compression, and the greater the compression magnitude, the more likely that nonlinear aspects of wave propagation lead to shock formation. However, they also show that the propagation velocity may be quickly damped as it propagates radially.

2.8. Impulse Propagation: Comparison With Data

[32] At the time of the sudden commencement, GOES 6 and 7 were at approximately 2032 MLT and 1840 MLT, respectively. Araki *et al.* [1997] show that there was a 17 s time lag for the onset of the pulse at these two satellites, implying a propagation speed of no more than 1090 km/s, generally slower than the 1000–2500 km/s values of the v_0 parameter used in our model. However, there is an important distinction to be made between this parameter and the actual velocity of the perturbation at a given point. The propagation velocity parameter in our model, v_0 , corresponds to the radial velocity at the point of impact. Also included is an azimuthal delay time, such that the velocity relevant for comparison is not radial velocity, except at the point of impact. The actual disturbance velocity at any point should be determined by the propagation of the electric field wavefront. Figure 2 shows the propagation of this wavefront (incoming pulse only) at 5 s time intervals. The positions of GOES 6 and 7 at the time of the event are marked by the star symbol. The time delay between the arrival of the model wavefront at the GOES satellites’ positions is approximately 12 s, which implies a velocity of 1544 km/s for $v_0 = 2000$ km/s. While this differs from the Araki *et al.* observation, it is closer than the comparison to the radial velocity parameter alone might imply. Using $v_0 = 1400$ km/s, we get essential agreement with the Araki *et al.* observation and still a substantial radiation belt though at a slightly lower energy than was observed. A possible description of this particular event includes shock-type propagation at higher L , slowing to fast-mode propagation at lower L , particularly in the plasmasphere. Looking at the wavefront propagation, although the radial velocity parameter does not explicitly vary with radial distance, we can see that the effective wavefront propagation velocity slows as it reaches lower L , which is more consistent with the basic physical picture. Also, the velocity of the pulse between the GOES satellites may not be so relevant because the most energized electrons do not pass close to those satellites, due

to the local time dependence of the impulse (see the dashed trajectory in Figure 2).

3. Summary

[33] On the basis of the Li *et al.* [1993] model used to explain the 24 March 1991 energetic electron injection event, our parametric study explored the effect of varying electric field amplitudes and magnetospheric propagation velocities on the shock-induced radial transport of radiation belt electrons. A larger amplitude pulse energizes electrons more and moves them closer to the Earth. However, this trend asymptotes, such that significantly increasing the electric field amplitude from the value of 240 mV/m used in modeling the 24 March 1991 event would not significantly shift the final position of energized electrons toward the Earth. A slower pulse propagation velocity results in the appearance of a peak closer to the Earth due to the dropoff of the contribution of electrons originally at higher L shells. However, because the electrons that contribute to the final peak interact with a slower impulse and are energized closer to the Earth, the final energy distribution is peaked at a lower energy. In addition, the flux level of very energetic electrons drops off sharply below a wave propagation velocity of about 1200 km/s.

[34] Use of a fast velocity in modeling fast mode propagation can be supported by comparison to MHD simulations of the impulse traveling at 1700 km/s, which is faster than the average local Alfvén speed. The Alfvén velocity falls off with radial distance within and outside of the plasmopause, such that it is well below modeled velocities necessary to energize particles to the observed levels in the region ($>7R_E$) from which most of the energized electrons come.

[35] Resonance of the propagating pulse with existing electron populations determines the impact an interplanetary shock will have on our Earth’s space environment. The 24 March 1991 event was unique because of the fast velocity of propagation through the magnetosphere and because of its large amplitude, probably due to an extremely sharp solar wind density or velocity increase. These features of the shock explain the high count rate at high energies observed by CRRES. The resonant nature of the process, and the importance of an existing population in the outer L -shells fulfilling the resonance conditions is emphasized by the result that propagation speeds of less than about 1200 km/s produce no new significant electron fluxes deep in the inner magnetosphere (L near 2.5) in the highly relativistic electron energy ranges, under our model.

[36] **Acknowledgments.** We thank both reviewers for their constructive comments and suggestions. This work was supported in part by NASA grants (NAG5-13135 and -13518) and NSF grants (CISM and ATM-0233302).

[37] Lou-Chuang Lee thanks Tohru Araki and Mary K. Hudson for their assistance in evaluating this paper.

References

- Albert, J. M. (2002), Nonlinear interaction of outer zone electrons with VLF waves, *Geophys. Res. Lett.*, *29*(8), 1275, doi:10.1029/2001GL013941.
- Araki, T., *et al.* (1997), Anomalous sudden commencement on March 24, 1991, *J. Geophys. Res.*, *102*, 14,075.
- Baker, D. N., S. G. Kanekal, X. Li, S. P. Monk, J. Goldstein, and J. L. Burch (2004), An extreme distortion of the Van Allen belt arising from the “Hallowe’en” solar storm in 2003, *Nature*, *432*, 878–881.

- Blake, J. B., W. A. Kolasinski, R. W. Rillius, and E. G. Mullen (1992), Injection of electrons and protons with energies of tens of MeV into $L < 3$ on March 24, 1991, *Geophys. Res. Lett.*, *19*, 821.
- Blake, J. B., P. L. Slocum, J. E. Mazur, M. D. Looper, and R. S. Selesnick (2005), Geoeffectiveness of shocks in populating the radiation belts, in *Multiscale Coupling of Sun-Earth Processes*, edited by A. T. Y. Liu, Y. Kamide, and G. Consolini, p. 125, Elsevier, New York.
- Elkington, S. R., M. K. Hudson, M. J. Wiltberger, and J. G. Lyon (2002), MHD/particle simulations of radiation belt dynamics, *J. Atmos. Sol. Terr. Phys.*, *64*, 607.
- Gannon, J. L., and X. Li (2005), Electron phasespace density analysis based on test-particle simulations of magnetospheric compression events, in *Particle Acceleration in Astrophysical Plasmas: Geospace and Beyond*, *Geophys. Monogr. Ser.*, vol. 156, edited by D. Gallagher et al., pp. 205–214, AGU, Washington, D. C.
- Horne, R. B., and R. M. Thorne (1998), Potential waves for relativistic electron scattering and stochastic acceleration during magnetic storms, *Geophys. Res. Lett.*, *25*, 3011.
- Hudson, M. K., A. D. Kotelnikov, X. Li, I. Roth, M. Temerin, J. Wygant, J. B. Blake, and M. S. Gussenhoven (1995), Simulation of proton radiation belt formation during the March 24, 1991 SSC, *Geophys. Res. Lett.*, *22*, 291.
- Hudson, M. K., S. R. Elkington, J. G. Lyon, V. A. Marchenko, I. Roth, M. Temerin, J. B. Blake, M. S. Gussenhoven, and J. R. Wygant (1997), Simulations of radiation belt formation during storm sudden commencements, *J. Geophys. Res.*, *102*, 14,087.
- Kantrowitz, A., and H. E. Petschek (1966), MHD characteristics and shock waves, *Plasma Physics in Theory and Application*, edited by W. B. Kunkel, pp. 147–199, McGraw-Hill, New York.
- Kennel, C. F., J. P. Edmiston, and T. Hada (1985), A quarter century of shock research, in *Collisionless Shocks in the Heliosphere*, *Geophys. Monogr. Ser.*, vol. 34, edited by R. G. Stone and B. T. Tsurutani, pp. 1–36, AGU, Washington, D. C.
- Kunkel, W. B., and M. N. Rosenbluth (1966), Introduction to plasma physics, *Plasma Physics in Theory and Application*, edited by W. B. Kunkel, pp. 2–20, McGraw-Hill, New York.
- Lee, D.-H., and M. K. Hudson (2002), Propagation of sudden impulses in the magnetosphere: Linear and nonlinear waves, in *Space Weather Study Using Multipoint Techniques*, *COSPAR Colloq. Ser.*, vol. 12, p. 175, Elsevier, New York.
- Li, X., and M. Temerin (2001), The electron radiation belt, *Space Sci. Rev.*, *95*, 569.
- Li, X., I. Roth, M. Temerin, J. Wygant, M. K. Hudson, and J. B. Blake (1993), Simulation of the prompt energization and transport of radiation particles during the March 24, 1991 SSC, *Geophys. Res. Lett.*, *20*, 2423.
- Li, X., M. K. Hudson, J. B. Blake, I. Roth, M. Temerin, and J. R. Wygant (1996), Observation and simulation of the rapid formation of a new electron radiation belt during March, 24, 1991 SSC, in *Workshop on the Earth's Trapped Particle Environment*, *AIP Conf. Proc.*, vol. 383, p. 109, AIP Press, Woodbury, N. Y.
- Li, X., D. N. Baker, S. Elkington, M. Temerin, G. D. Reeves, R. D. Belian, J. B. Blake, H. J. Singer, W. Peria, and G. Parks (2003), Energetic particle injections in the inner magnetosphere as a response to an interplanetary shock, *J. Atmos. Sol. Terr. Phys.*, *65*, 233.
- Li, X., M. Temerin, B. T. Tsurutani, and S. Alex (2005), Modeling the 1–2 September 1859 super magnetic storm, *Adv. Space Res.*, in press.
- Looper, M. D., J. B. Blake, and R. A. Mewaldt (2005), Response of the inner radiation belt to the violent Sun-Earth connection events of October/November 2003, *Geophys. Res. Lett.*, *32*, L03S06, doi:10.1029/2004GL021502.
- Lorentzen, K. R., J. E. Mazur, M. D. Looper, J. F. Fennell, and J. B. Blake (2002), Multisatellite observations of MeV ion injections during storms, *J. Geophys. Res.*, *107*(A9), 1231, doi:10.1029/2001JA000276.
- Meredith, N. P., R. B. Horne, and R. R. Anderson (2001), Substorm dependence of chorus amplitudes: Implications for the acceleration of electrons relativistic energies, *J. Geophys. Res.*, *106*, 13,165.
- Meredith, N. P., R. B. Horne, R. H. Iles, R. M. Thorne, D. Heynderickx, and R. R. Anderson (2002), Outer zone relativistic electron acceleration associated with substorm enhanced whistler mode chorus, *J. Geophys. Res.*, *107*(A7), 1144, doi:10.1029/2001JA900146.
- Northrop, T. G. (1963), *The Adiabatic Motion of Charged Particles*, Interscience, New York.
- Schulz, M., and L. Lanzerotti (1974), *Particle Diffusion in the Radiation Belts*, Springer, New York.
- Selesnick, R. S., J. B. Blake, W. A. Kolasinski, and T. A. Fritz (1997), A quiescent state of 3 to 8 MeV radiation belt electrons, *Geophys. Res. Lett.*, *24*, 1343.
- Summers, D., R. M. Thorne, and F. Xiao (1998), Relativistic theory of wave-particle resonant diffusion with application to electron acceleration in the magnetosphere, *J. Geophys. Res.*, *103*, 20,487.
- Temerin, M., I. Roth, M. K. Hudson, and J. R. Wygant (1994), New paradigm for the transport and energization of radiation belt particles, *Eos Trans. AGU*, *75*(44), Fall Meet. Suppl., F538.
- Tsurutani, B. T., W. D. Gonzalez, G. S. Lakhina, and S. Alex (2003), The extreme magnetic storm of 1–2 September 1859, *J. Geophys. Res.*, *108*(A7), 1268, doi:10.1029/2002JA009504.
- Waters, C. L., B. G. Harrold, F. W. Merik, J. C. Samson, and B. J. Fraser (2000), Field line resonances and waveguide modes at low latitudes, *J. Geophys. Res.*, *105*, 7763.
- Wilken, B., C. K. Goertz, D. N. Baker, P. R. Higbie, and T. A. Fritz (1982), The SSC on July 29, 1977 and its propagation within the magnetosphere, *J. Geophys. Res.*, *87*, 5901.
- Wygant, J., F. Mozer, M. Temerin, J. Blake, N. Maynard, H. Singer, and M. Smiddy (1994), Large amplitude electric and magnetic field signatures in the inner magnetosphere during injection of 15 MeV electron drift echoes, *Geophys. Res. Lett.*, *21*, 1739.

J. L. Gannon and X. Li, Laboratory for Atmospheric and Space Physics, University of Colorado, 1234 Innovation Drive, Boulder, CO 80303, USA. (gannonjl@colorado.edu)

M. Temerin, Space Sciences Laboratory, University of California, Berkeley, Centennial Drive at Grizzly Peak Blvd., Berkeley, CA 94720, USA.